Random interfaces generated by the addition of structures of variable size

Nicolas Pétrélis
Laboratoire Jean Leray, Université de Nantes, 2, Rue de la Houssinière, 44322 Nantes Cedex 3, Nantes, France

François Pétrélis
Laboratoire de Physique de l'Ecole Normale Supérieure, ENS, Université PSL, CNRS, Sorbonne Université, Université Paris-Diderot, Paris, France

(Received 30 July 2023; revised 19 September 2024; accepted 4 November 2024; published 24 December 2024)

We consider the random deposition of objects of variable width and height over a line. The successive additions of these structures create a random interface. We focus on the regime of heavy-tailed distributions of the structure width. When the structure center is chosen at random, the problem is exactly solvable, and the interface generically tends toward a self-affine random curve. The asymptotic behavior reached after a large number of iterations is universal in the sense that it depends on only three parameters: the shape of the added structure at its maximum, the power-law exponent of the width distribution, and the exponent that relates height and width. The parameter space displays several transitions that separate different asymptotic behaviors. In particular, for a set of parameters, the interface tends toward a fractional Brownian motion. Our results reveal the existence of a new class of random interfaces whose properties appear to be robust. The mechanism that generates correlations at large distances is identified, and it explains the appearance of such correlations in several situations of interest, such as the physics of earthquakes or the propagation of energy through a diffusive medium.

DOI: 10.1103/PhysRevE.110.064804

The evolution of an interface that is modified by the successive addition of objects is an iconic problem in statistical physics, with applications ranging from the deposit of a granular [1] to the growth of a stable phase into a metastable one, or to the propagation of a flame to quote a few [2]. In the past decades, the competition between randomness and diffusion was shown to be modeled by the Edwards-Wilkinson (EW) equation and, when nonlinearity is taken into account, by the Kardar-Parisi-Zhang (KPZ) equation [3]. The quest for their understanding drove a variety of efforts both on the theoretical front [4] and the experimental one [5]. The additive term in these equations is a Gaussian white noise both in time and space and is thus uncorrelated. In a one-dimensional (1D) geometry, the solutions tend at long times toward a Brownian motion [2]. A Gaussian and correlated noise has also been considered [6].

Very few studies consider the case of the random addition of objects of varying size, and they are restricted to either a binary size distribution [7] or a Poisson one [8]. Here, we consider objects that have a heavily tailed distribution of size and show that such a process leads to a new class of random interfaces displaying various behavior. Notably, spatial correlations at large distances appear even when the individual steps of the process are uncorrelated.

The initial motivation for this problem comes from the physics of earthquakes (EQs) [9]. We will thus describe the models in this context. However, the addition of objects of variable size is a general situation, and applications in the context of the interaction of a wave with a diffusive medium are given at the end of this article.

We have shown in several models that the statistical properties of the EQ result from the stress field being a self-affine random curve [9]. More precisely, in a 1D geometry, the large scales of the stress field tend toward a Brownian motion or a fractional Brownian motion (fBm). This property originates in the stress field evolution that results from the successive stress changes caused by the EQ. The mechanism is the following iterative sequence: the stress field at a given time controls the properties of the next EQ and, in particular, the amount of slip caused by the event; the slip is in turn responsible for the modification of the stress. After a large number of iterations, this process builds up a self-affine stress field. We identified this process in several models and showed that it is responsible for the intriguing properties of EQs [9,10], such as the distribution of the released energy (the Gutenberg-Richter law) or the distribution of aftershocks after a main shock (the Omori law). It is thus expected that this process is generic, robust, and can be observed in idealized models of EQs. Nevertheless, the origin of the large distance correlations, as displayed by the self-affine stress field, is unclear. The purpose of this article is to identify why and when such large distance correlations appear. To achieve this goal, we consider two models, rigorously solve one of them, and study them numerically.

The simplest model of the evolution of a stress field is to consider that it is a scalar function of space and that successive EQs change its value. Between events, the stress increases due to tectonic loading, which is usually considered to be spatially uniform and linear in time. When the stress reaches a threshold, an EQ is initiated. After the event, the stress in the domain that has moved is decreased.

To deal with positive quantities, we define $h(x)$ as the opposite of the stress and assume that each event results in the addition of a value $\delta h(x)$ to $h(x)$. The linear in time loading between events is not considered here, as it only amounts to

a change in the spatial average of h. The problem is thus turned into the evolution of an interface $h(x)$ that drifts toward positive values because of the successive deposition of objects that change its value by a quantity $\delta h(x)$.

An EQ affects the fault property over a size that is distributed as a power law [9,12], and we thus assume that δh is nonzero over a width similarly distributed.

We consider two variations of this process. EQs are usually initiated at locations at which the stress is maximum, which corresponds to the minimum value of h: this is the min-model. We also consider a simpler situation, the rand-model, in which the stress drop or equivalently the change in h occurs at a random position, independent of the value of h.

In a more formal way, we consider positions on a line $x \in [0, D]$. We use periodic boundary conditions to maintain homogeneity in the statistical properties of the system. We are interested in $h_N(x)$ the height after N iterations. An iteration consists of the addition of $\delta h(x)$ defined as follows: Let $\psi : [0, 1] \mapsto \mathbb{R}^+$ be a continuous function, such that $\psi(0) = 1$ and $\psi(1) = 0$, and let n be the index of its first nonzero derivative at 0^+. For $n = 1$, ψ is locally a triangle, and for $n = 2$ a parabola. Let s be the center of the structure that is either drawn at random over $[0, D]$ for the rand-model or is the minimum of $h(x)$ for the min-model. Let U be the width of the structure. It is a random variable distributed as a Pareto law with parameter $\beta - 1$ ($\beta > 1$), that is, with density $1_{[1,\infty)}(u)(\beta - 1)/u^\beta$. Let $v_s(x) = \min\{|s - x + jD|, j \in \mathbb{Z}\}$ be the distance between the center and the position x, where we use the periodicity of the system. We then define

$$\delta h(x) = U^{\alpha-1}\, 1_{[0,U[}(v_s(x))\, \psi\left(\frac{v_s(x)}{U}\right). \tag{1}$$

In other words, at each iteration, we add a structure of shape ψ, of width $2U$, and of amplitude $U^{\alpha-1}$. The structure is even with respect to its center, and its width is random and distributed as a power law of exponent $-\beta$.

These processes can be simulated numerically, and we display in Fig. 1 profiles of $h = h_N(x)$ calculated over a grid of spacing $\Delta x = 1$ when ψ is linear so that the added structure is a triangle ($n = 1$).

For both models, several results can be proven rigorously using probabilistic methods applied to random curves. Details are provided in the Appendix but we focus here on the results. Interestingly, they depend exclusively on n, α, and β.

The spatial average of h increases with N either linearly (ballistic) for $\beta > \alpha$ or as $N^{\frac{\alpha-1}{\beta-1}}$ (superballistic) for $\beta < \alpha$. More precise estimates are given in Eqs. (A4), (A5), and (A6).

For the rand-model, we are able to fully describe the spatial fluctuations in h. Let $f_N(x) = h_N(x) - h_N(0)$.

(1) For $\alpha > 1 + n$ and $1 < \beta \leqslant \beta_c := 2\alpha - 1 - 2n$,

$$N^{-\frac{\alpha-1-n}{\beta-1}} f_N \Rightarrow_N \mu, \tag{2}$$

where μ is the distribution of a random function, which can be expressed as the limit of a sum of random functions, see Eqs. (2), (A8), and (A9). In particular, the fluctuations in h are not a Gaussian process.

(2) For $\alpha \in [1, 1 + n]$ or for $\alpha > 1 + n$ and $\beta > \beta_c$,

$$N^{-\frac{1}{2}} f_N \Rightarrow_N Y, \tag{3}$$

where Y is a centered Gaussian process.

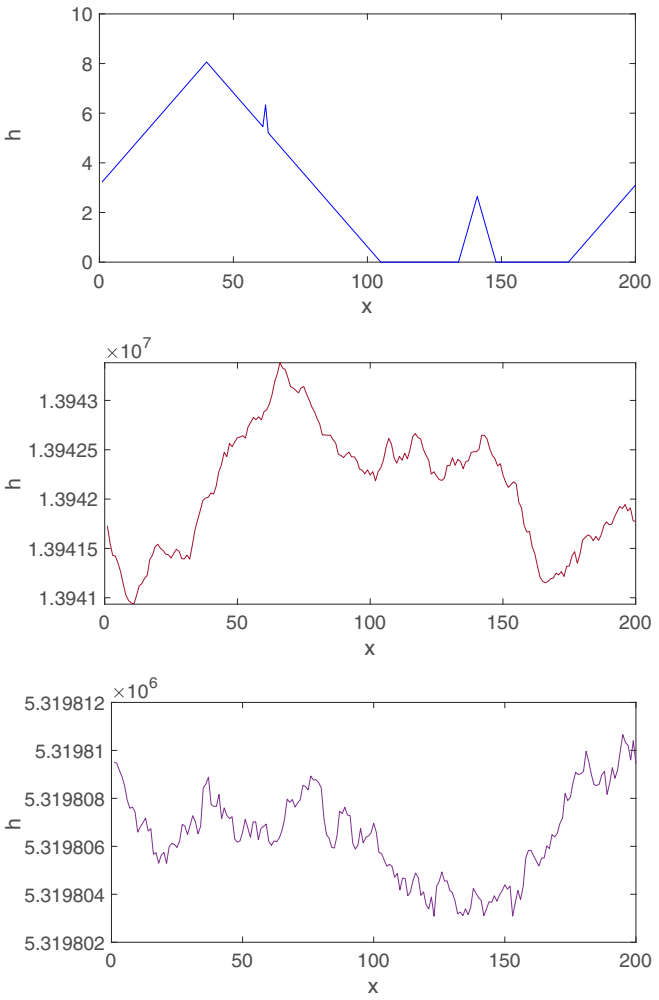

FIG. 1. Numerically simulated interface $h(x) = h_N(x)$ for a segment of length $D = 200$, $\alpha = 1.5$, and $\beta = 1.5$. Top: rand-model after $N = 3$ iterations starting from a straight line. Middle: rand-model after $5\,10^5$ iterations. Bottom: min-model after $5\,10^5$ iterations.

In this case, we are able to derive an analytical expression for the covariance $r(s, t) = \mathrm{Cov}\,(Y(s), Y(t))$. We verified by estimating the quantities numerically that for $\beta \geqslant \beta_f := 2\alpha - 2$ and for $D \gg s, t \gg 1$, $r(s, t) \propto |s|^{2H} + |t|^{2H} - |s - t|^{2H}$ with $2H = 2\alpha - \beta$. When $\beta \leqslant \beta_f$, the covariance is dominated by quadratic terms in s or t.

We draw the parameter space of the rand-model in Fig. 2. It contains three transitions separating six different behaviors.

A particularly interesting regime concerns $0 \leqslant 2\alpha - \beta \leqslant 2$. Then the process generates a fBm of Hurst exponent H with

$$H = \alpha - \beta/2\,. \tag{4}$$

The value of the Hurst exponent can be understood as follows: The difference in height $\langle f_N(l)^2 \rangle$ between two sites distant of l is due to events of size L larger than l, whose center is within a neighborhood of one of the two sites over a width proportional to l. These events provide a height difference of order $l^{\alpha-1}$. When the integral is dominated by the smaller values of L, we

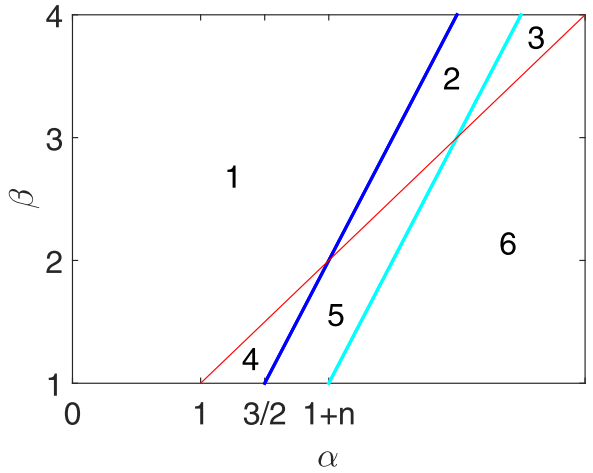

FIG. 2. Parameter space describing the behavior of the interface $h_N(x)$ at large N for the rand-model. The red line is $\beta = \alpha$ and separates between a ballistic (domain 1, 2, and 3) and a superballistic (4, 5, and 6) behavior of the mean position of the interface. The cyan line is $\beta_c = 2\alpha - 1 - 2n$ and separates between a Gaussian (1, 2, 4, 5) and a non-Gaussian (3, 6) behavior of the field fluctuations. The blue line is $\beta_f = 2\alpha - 2$ and separates between a $x^{2\alpha-\beta}$ behavior (1 and 4) of the correlations of the fluctuations and a x^2 one (2, 3, 5, 6).

obtain the estimate

$$\langle f_N(l)^2 \rangle \simeq l\, l^{2\alpha-2} \int_l^\infty L^{-\beta} dL \simeq l^{2\alpha-\beta}.$$

It is worth noting that this result does not depend on n, and is thus independent of the shape of the added structures.

Examples of profiles are presented in Fig. 3. We calculate from these profiles the power spectrum density (PSD) of $f_N/N^{1/2}$. The power law of the PSD, K^{-1-2H} for a fBm, allows for calculation of H, which is displayed in Fig. 4. It verifies the prediction of Eq. (4).

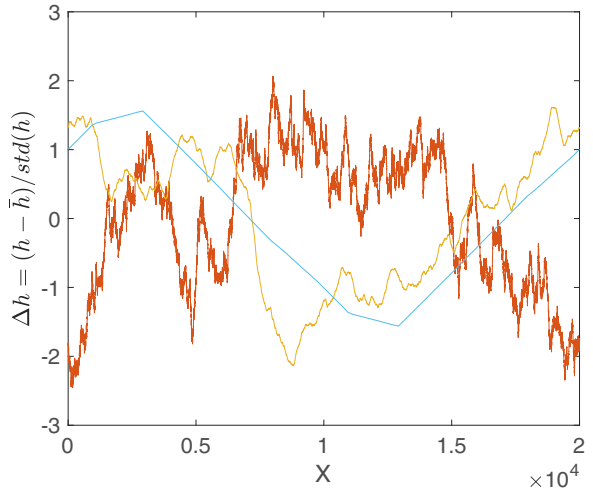

FIG. 3. For the rand-model and $\beta = 2$, normalized height profile as a function of position after $N = 10^7$ iterations for a triangular added structure ($n = 1$) and (red) $\alpha = 1.5$, (yellow) $\alpha = 2$, and (light blue) $\alpha = 3$.

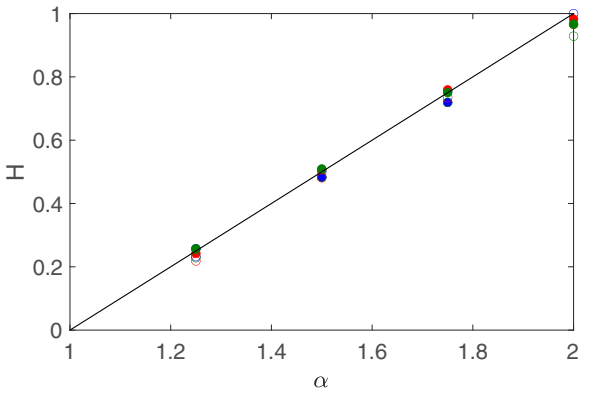

FIG. 4. Hurst exponent H as a function of α for $\beta = 2$. The straight line is the prediction $H = \alpha - \beta/2$. Full symbols are the results of the rand-model and empty symbols of the min-model. Red is for $n = 1$ (triangle), blue for $n = 2$ (parabola), and green for $n = 2$, parabolic at its center with a negative value of δh at its border.

Notably, the phenomenology differs from that of the KPZ solutions in 1D, which tend toward a Brownian motion (with $H = 1/2$) when the noise term is uncorrelated [2] or that transitions between a Brownian motion and a long-range correlated regime (with $H > 1/2$) when the noise term is Gaussian and its correlation at long range is increased [6]. Therefore, the models we present here belong to a different universality class.

The min-model is a challenging problem for its theoretical aspects, as the dynamics relies on a nonlocal constraint. The results for the spatial average of h are the same as for the rand-model. For the fluctuations, we must rely on numerical simulations, see Fig. 1 (bottom). We focus here on the regime $0 < 2\alpha - \beta \leqslant 2$, for which the rand-model generates a fBm. In contrast to the rand-model, the moments of fluctuations do not increase with N but remain bounded. The skewness is small but nonzero, the flatness is slightly smaller than 3, the value for a Gaussian. It increases with the size D. It is quite interesting that the application of the min rule for finding the location of the next EQ is sufficient to saturate the growth with the number of iterations of the moments of the fluctuations of the stress profile.

The value of H obtained from the PSD is displayed in Fig. 4. As for the rand-model, the results are very close to the prediction of Eq. (4). The H-exponent is thus independent of the shape of the added structure and the nature of the model (rand or min).

In the models considered here, the spatial structure of the stress change is the same at each event, up to a change in its width and height. The shape, width, and height are independent of h, whereas in a fault, it is the spatial variations in h that determine the slip, which controls the change in stress. The independence of stress change on the stress (for the rand-model) or of only dependence for its center set by the stress maximum (for the min-model) are simplifications that allow for theoretical progress. Yet, the observed phenomenology is rich and similar to that observed in more realistic models [9,10]. In particular, our results explain why the random addition of structures of variable size generically gen-

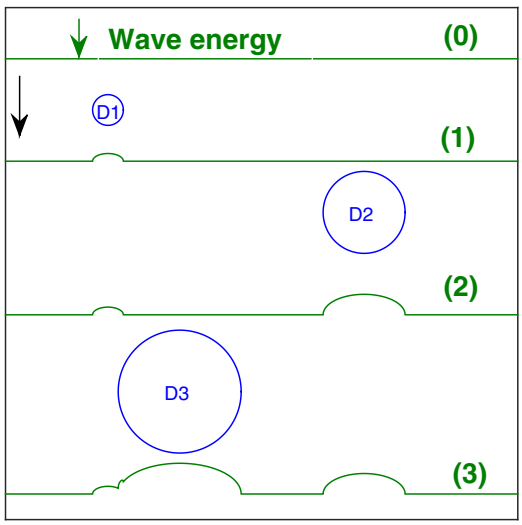

FIG. 5. Schematics of the variation of a plane wave that propagates in a straight line from the top to the bottom parallel to the black arrow. The wave energy is displayed as a green line. It is decreased at each interaction with an absorbing object D_i sketched as a blue circle and proportionally to the width of the absorber in the direction of propagation. The energy after the (i)-th encounter is displayed for $i = 0$ to 4.

erates self-affine behavior. In the context of EQ physics, this phenomenon provides a possible explanation for the appearance of large distance correlations of the stress field.

Several observations in natural data are consistent with our description. It is well known that EQ areas are distributed as a power law with exponent β_a close to 2 [11–14]. This amounts to a distribution of the length of the EQ with power-law exponent $\beta \simeq 3$. In addition, the stress change at each event is independent of its length so that α is of order 1 [12]. Regarding the existence of large-scale correlations, the topography of faults is self-affine with their roughness associated with a Hurst exponent of order 0.2 to 0.8 [15]. In addition, evidence suggests that the slip itself scales with a Hurst exponent close to 0.6. Using a three-dimensional fault numerical model, it was predicted that the two-dimensional frictional stress field scales with a Hurst exponent of -0.4 [16]. All these fields in nature thus display correlations at large scale.

This new class of random interfaces is of interest for the physics of EQs, but also as a new stochastic process, different from the ones generated by the EW or KPZ equations. It has possible applications in a variety of domains. For instance, the deposition of polymers of variable size is expected to belong to this new class, provided the polymer size has a wide distribution. Another application of broad interest, which might at first sight appear quite unrelated, is the propagation of a wave through a medium containing objects of variable size. Consider the energy of a plane wave that propagates in a straight line and study its evolution when it interacts with a set of objects that absorb partially the wave energy. When the absorption is proportional to the length of the path of the wave in the object, the wave energy after the object is decreased by a quantity proportional to the width of the object along the path of the wave. This is sketched in Fig. 5. The interaction of the wave with a set of absorbers amounts to the sum of the interaction with each one. Therefore the expression for the variation of the wave energy is given by the same formula as the variation of the stress profile in Eq. (1). The results obtained here apply to the wave energy identically.

Several applications come to mind. Fragmentation processes often produce collections of objects with size distributed as a power law [17]. This can be the case for drops fragmented in a turbulent flow [18]. An experiment using two fluids matched in index and such that drops of one of the two phases absorb the light at a given frequency would realize the situation in Fig. 5 [19]. A second system relies on aerosols in the atmosphere, which have a size distribution that can be large [20], and in some situations is modeled by the Junge law [21], a power-law distribution generated by coagulation processes [22]. We expect that the absorption of light or of UV rays through such an aerosol cloud results in energy transmission that varies in the plane perpendicular to the direction of propagation. In the idealized limit where we neglect scattering processes, the energy spatial variation in the perpendicular plane is exactly obtained by the rand-model. Our results indicate that the pattern of energy should display a self-affine behavior with properties controlled by the distribution of the size of the aerosols, and it would be interesting to investigate how this is affected when scattering cannot be neglected. Finally, we describe a third example related to the propagation of electromagnetic energy through the universe. Interstellar clouds are domains where the density is large. These clouds are magnetized, and their emission at microwave frequencies is polarized. The statistical characterization of this interstellar emission is of prime importance to experiments exploring the signature of primordial gravitational waves in the cosmic microwave background polarization. It has been shown that a source term assumed to be a correlated Gaussian field with a prescribed Hurst exponent leads to a realistic pattern [23]. Our results for the rand-model provide a possible explanation for the origin of this spatially correlated source term: It would result from the addition of randomly distributed interstellar clouds whose radius are actually known to be distributed as a power law [24].

The rand-model is thus expected to explain the behavior of systems in various contexts ranging from the absorption of light by two-phase turbulent flows or by aerosols to the microwave emission by interstellar clouds. Further work will extend the results presented here to two-dimensional geometry and obtain quantitative predictions.

We thank Bernard Legras for discussions related to absorption by aerosols and Francois Boulanger for discussions and raising our attention to the problem of emission at microwave frequency by interstellar clouds.

APPENDIX

In this Appendix, several results presented in the manuscript are described rigorously and justified at a heuristic level. We also provide formulas not presented in the article. In particular, our aim is to prove that, as the number of random transformations N becomes large, the front h_N and its fluctuations, both rescaled with an *ad-hoc* power of N,

resemble the typical trajectory of a well-identified limiting random process. Deriving these results requires settling some notations. This is done in subsection A. We present the results for the mean position of the front in subsection B and the fluctuations in subsection C. We combine a rigorous mathematical presentation with short descriptions adequate for physicists.

1. Definition

We first need to define the notion of convergence of a random process and, in particular, the convergence in distribution. To that aim, we denote by C the set of continuous real functions on $[0, D]$, by $||\cdot||_\infty$, the norm of the uniform convergence on $[0, D]$, and by $\mathcal{C}$, the associated Borel σ-algebra. For μ, a probability law on $(C, \mathcal{C})$ and for $(X_n)_{n\geqslant 1}$ a sequence of random continuous functions (defined on a probability space $(\Omega, \mathcal{A}, P)$), we will set

$$X_n \Rightarrow_n \mu \tag{A1}$$

when X_n converges in distribution in $(C, \mathcal{C})$ toward μ as $n \to \infty$. By extension, if X is a random continuous function, we will set $X_n \Rightarrow_n X$ if X_n converges to the law of X as $n \to \infty$. This convergence can be understood as follows: Consider any bounded continuous functional $g : (C, ||\cdot||_\infty) \mapsto \mathbb{R}$. The latter convergence means that

$$\lim_{n\to\infty} \int_\Omega g(X_n(\omega))dP(\omega) = \int_\Omega g(X(\omega))dP(\omega).$$

This is what mathematicians call convergence in distribution.

Proving rigorously a convergence of type (A1) on $(C, \mathcal{C})$ requires the use of mathematical tools from [25], Chapter 2 or [26], Theorem 21.42. There are two hypotheses to verify to conclude that $X_n \Rightarrow_n X$:

(1) The convergence in finite dimensional distributions of X_n toward X. To that aim, for $0 \leqslant t_1 < t_2 < \cdots < t_k \leqslant 1$, one has to check that the random vector $(X(t_1), \ldots, X(t_k))$ is the limit in distribution of the sequence $(X_n(t_1), \ldots, X_n(t_k))_{n\geqslant 1}$. We note that this is equivalent to the property that the Fourier transform of the vector $(X_n(t_1), \ldots, X_n(t_k))$ converges as $n \to \infty$ toward the Fourier transform of $(X(t_1), \ldots, X(t_k))$.

(2) The tightness of $(X_n)_{n\geqslant 1}$ in $(C, ||\cdot||_\infty)$, which provides, with a probability arbitrarily close to 1, a uniform (in n) control on the modulus of continuity of X_n that is of its fluctuations (in t). This tightness is, for instance, obtained with the Kolmogorov criterion (stated in [25], Theorem 12.3) by proving that there exists a $C > 0$ such that for every $0 \leqslant s < t \leqslant 1$,

$$\sup_{n\geqslant 1} \int_\Omega |X_n(t, \omega) - X_n(s, \omega)|^2 dP(\omega) \leqslant C(t - s)^2.$$

Qualitatively, the process must have spatial variations that are not too large (uniformly in the number of iterations).

In summary, if X_n satisfies these two properties, then it converges in distribution toward X.

We also use the well-established equality in law between the order statistics of N independent Pareto-distributed random variables of parameter β and the random vector

$$\left(\left(\frac{T_{N+1}}{T_1}\right)^{\frac{1}{\beta-1}}, \ldots, \left(\frac{T_{N+1}}{T_N}\right)^{\frac{1}{\beta-1}}\right), \tag{A2}$$

where $T_0 = 0$ and $(T_{i+1} - T_i)_{i\geqslant 0}$ is a sequence of independent and identically distributed (i.i.d.) random variables following an exponential law of parameter 1. This, among other properties useful for physicists, implies that the largest values of N independent Pareto random variables are of order $N^{\frac{1}{\beta-1}}$. We will use this property to justify the behavior at large N of the front as given by Eq. (A4).

2. Mean position of the front

Let us be more specific by defining the process h_N. Let $(Z_i)_{i\geqslant 1}$ be a sequence of independent random variables following a Pareto distribution of parameter $\beta - 1$. Then, for the rand-model, we let $(Y_i)_{i\geqslant 1}$ be an i.i.d. sequence of random variables following a uniform law on $[0, D]$, whereas for the min-model, Y_i is the leftmost point on $[0, D]$ where the minimum of h_{i-1} is attained. Thus, we set for $N \geqslant 1$,

$$h_N(x) := \sum_{i=1}^{N} Z_i^{\alpha-1} 1_{[0,Z_i)}(v_{Y_i}(x))\, \psi\left(\frac{v_{Y_i}(x)}{Z_i}\right), \quad x \in [0, D]. \tag{A3}$$

We now present the results for the mean position of the front. In the case of $\beta < \alpha$, for both the random and the minimum processes,

$$N^{-\frac{\alpha-1}{\beta-1}}\, h_N \Rightarrow_N R, \tag{A4}$$

where R is a real random variable, which by abuse of notation is considered here as a random function in C that is constant on $[0, D]$. Moreover, R follows a $\frac{\alpha-1}{\beta-1}$ stable law of characteristic function

$$\Phi(t) = \frac{\beta - 1}{2\alpha - \beta - 1} \exp\left[\Gamma\left(-\frac{\beta - 1}{\alpha - 1}\right)|t|^{-\frac{\beta-1}{\alpha-1}} + i\,\frac{\pi\,(\beta - 1)}{2\,(\alpha - 1)}\right]. \tag{A5}$$

In the case of $\beta > \alpha$, we obtain

$$N^{-1}\, h_N \Rightarrow_N 2\,\frac{\beta - 1}{D}\left[\int_0^1 \psi(u)\,du \int_1^{D/2} z^{\alpha-\beta} dz + \int_{D/2}^{\infty} z^{\alpha-1-\beta} \int_0^{D/2} \psi\left(\frac{y}{z}\right) dy dz\right], \tag{A6}$$

that is to say, the limit is a nonrandom constant function on $[0, D]$. The critical case $\beta = \alpha$ can also be analyzed rigorously, and for both the rand- and the min-model, the following convergence holds true:

$$(N\,\log N)^{-1}\, h_N \Rightarrow_N 1,$$

where, as in the latter case, the convergence takes place toward a nonrandom constant function that equals 1 on $[0, D]$. Let us give a heuristic for the growth rate of the front (as a function of N) that becomes ballistic for β larger than α. Recall Eq. (1) of the article and observe that when $\beta > \alpha$, the increments are integrable since $Z^{\alpha-1}$ has a finite first moment. For this

reason, the law of large numbers can be applied to the spatial average of both the rand- and the min-models, which equal a sum of independent identically distributed random variables (the integrals of the increments). As a consequence the spatial average of h_N grows linearly in N. In the case of $\alpha > \beta$, we note that $Z^{\alpha-1}$ is a nonintegrable heavy-tailed random variable, and so are the increments of the front. As a consequence, the law of large numbers is not applicable anymore. However, the characterization of the order statistics of $(Z_1, \ldots, Z_N)$ displayed in Eq. (A2) allows us to assert that the sum in Eq. (A3) is dominated by its k largest increments, provided k is chosen large enough (but finite and not dependent on N). This explains the convergence in Eq. (A4) and in particular, the superballistic rescalling in $N^{\frac{\alpha-1}{\beta-1}}$.

3. Fluctuations

For the rand-model, we are able to fully describe the fluctuations in h. We set $f_N(x) = h_N(x) - h_N(0)$.

(1) For $\alpha > 1 + n$ and $1 < \beta \leqslant \beta_c := 2\alpha - 1 - 2n$,

$$N^{-\frac{\alpha-1-n}{\beta-1}} f_N^r \Rightarrow_N \mu, \tag{A7}$$

where μ is the limiting law on $(C, \mathcal{C})$ of the sequence of continuous processes $(\gamma_N)_{N\in\mathbb{N}}$ defined as

$$\gamma_N(x) := \sum_{i=1}^{N} \frac{G_i(x)}{T_i^{\frac{\alpha-1-n}{\beta-1}}}, \quad x \in [0, D], \tag{A8}$$

where for $x \in [0, D]$,

$$G_i(x) := \frac{\psi^{(n)}(0)}{n!}(v_{Y_i}(x)^n - v_{Y_i}(0)^n), \tag{A9}$$

where $(Y_i)_{i\in\mathbb{N}}$ is a sequence of i.i.d. random variables following a uniform law on $[0, D]$. Observe that we used the results of Eq. (A2) to obtain Eq. (A8). Note also that the convergence of $(\gamma_N)_{N\geqslant 1}$ occurs almost surely if $\alpha - 1 - n > \beta - 1$, that is, $\beta < \alpha - n$. The interest of this result is that Eqs. (2), (A8), and (A9) provide an explicit formula for calculating or simulating the asymptotic behavior of the front.

(2) For $\alpha \in [1, 1 + n]$ or $\alpha > 1 + n$ and $\beta > \beta_c$,

$$N^{-\frac{1}{2}} f_N^r \Rightarrow_N Y, \tag{A10}$$

where Y is a centered Gaussian process with covariance function $r(s, t) = \mathrm{Cov}\,(X_1(s), X_1(t))$. In the case of a triangle ($n = 1$), there exists a $C > 0$ such that

$$r(t, t) := \mathrm{Var}(X_1(t)) \leqslant C \max\{t^2,\ t^{2\alpha-\beta}\}, \quad t \in [0, D]. \tag{A11}$$

For the rand-model, the regime change for the growth rate of the fluctuations of the front occurs at β_c, because for $\beta > \beta_c$, we enter the domain of application of the central limit theorem. Again, with Eq. (1) of the article, we observe that, since n is the index of the first nonzero derivative of ψ at 0, the fluctuations of a single increment $\delta(h(x) - h(0))$ are bounded above and below by a constant time to $Z^{\alpha-1-n}$, which is square integrable for $\beta > \beta_c$ only.

Finally, let us give a short explanation of the fact that when $\beta > \beta_f = 2\alpha - 2$, the covariance $r(s, t)$ has an exponent $2\alpha - \beta > 2$. Let $s < t$. For both s and t to be affected by the transformation, it is necessary that $t - s \leqslant 2Z$. Moreover, $\beta > \beta_f$ implies $\beta > \beta_c$, so that $Z^{\alpha-1-n}$ is square integrable and $E[Z^{2(\alpha-1-n)}\, 1_{\{2Z\geqslant t-s\}}]$ behaves as $(t - s)^{2\alpha-\beta}$, which explains our result.

[1] S. F. Edwards and D. R. Wilkinson, Proc. R. Soc. London A **381**, 17 (1982).

[2] T. Halpin-Healy and Y. C. Zhang, Phys. Rep. **254**, 215 (1995).

[3] M. Kardar, G. Parisi, and Y. C. Zhang, Phys. Rev. Lett. **56**, 889 (1986).

[4] M. Hairer, Ann. Math. **178**, 559 (2013).

[5] K. A. Takeuchi, Physica A **504**, 77 (2018).

[6] H. K. Janssen, U. C. Täuber, and E. Frey, Eur. Phys. J. B **9**, 491 (1999).

[7] P. K. Mandal and D. Jana, Phys. Rev. E **77**, 061604 (2008).

[8] F. L. Forgerini and W. Figueiredo, Phys. Rev. E **79**, 041602 (2009).

[9] F. Pétrélis, K. Chanard, A. Schubnel, and T. Hatano, Phys. Rev. E **107**, 034132 (2023).

[10] F. Pétrélis, K. Chanard, A. Schubnel, and T. Hatano, J. Stat. Mech. (2024) 043404.

[11] C. H. Scholz, *The Mechanism of Earthquakes and Faulting* (Cambridge University Press, Cambridge, 2019).

[12] H. Kanamori and E. E. Brodsky, Rep. Prog. Phys. **67**, 1429 (2004).

[13] H. Kawamura, T. Hatano, N. Kato, S. Biswas, and B.K. Chakrabarti, Rev. Mod. Phys. **84**, 839 (2012).

[14] The magnitudes m of earthquake are distributed as an exponential $\exp -bm$ with b close to unity. m is proportional to $\log(S)$ where S is the size of the earthquake so that S is distributed as power-law of exponent close to -2.

[15] F. Renard *et al.*, Geophys. Res. Lett. **40**, 83 (2013); S. Abe and H. Deckert, Solid Earth **12**, 2407 (2021); L. Bruhat *et al.*, Geophys. J. Int. **220**, 1857 (2020).

[16] T. Candela *et al.*, Geophys. J. Int. **187**, 959 (2011).

[17] P. Krapivski *et al.*, *A Kinetic View of Statistical Physics* (Cambridge University Press, Cambridge, 2010).

[18] C. Garrett, M. Li, and D. Farmer, J. Phys. Oceanogr. **30**, 2163 (2000).

[19] S. Wiederseiner *et al.*, Exp. Fluids **50**, 1183 (2011).

[20] O. Boucher, *Atmospheric Aerosols* (Springer, Netherlands, 2015).

[21] C. Junge, J. Atmos. Sci. **12**, 13 (1955).

[22] C. White, J. Colloid Interface Sci. **87**, 204 (1982).

[23] Planck collaboration, Astron. Astrophys. **596**, A105 (2016).

[24] B. G. Elemegreen and E. Falgarone, Astrophys. J. **471**, 816 (1996).

[25] P. Billingsley, *Convergence of Probability Measures*, 2nd ed. (John Wiley & Sons Inc., New York, 1999).

[26] A. Klenke, *Probability Theory: A Comprehensive Course* (Springer, Cham, 2007).